UCSF

UC San Francisco Previously Published Works

Title

Chapter 23 Ratiometric Imaging of pH Probes

Permalink

https://escholarship.org/uc/item/7v5171qm

Authors

Grillo-Hill, Bree K
Webb, Bradley A
Barber, Diane L

Publication Date

2014

DOI

10.1016/b978-0-12-420138-5.00023-9

Peer reviewed

Methods in Cell Biology • Volume 123

QUANTITATIVE IMAGING
IN CELL BIOLOGY

Edited by
Jennifer C. Waters & Torsten Wittmann

CHAPTER

Ratiometric Imaging of pH Probes

23

Bree K. Grillo-Hill, Bradley A. Webb, Diane L. Barber

Department of Cell and Tissue Biology, University of California, San Francisco, California, USA

CHAPTER OUTLINE

Abstract

Measurement of intracellular pH can be readily accomplished using tools and methods described in this chapter. We present a discussion of technical considerations of various ratiometric pH-sensitive probes including dyes and genetically encoded sensors. These probes can be used to measure pH across physical scales from macroscopic whole-mount tissues down to organelles and subcellular domains. We describe protocols for loading pH-sensitive probes into single cells or tissues and discuss ratiometric image acquisition and analysis.

INTRODUCTION

Proton fluxes across cell membranes are regulated by extracellular and intracellular cues to drive many cell processes. Predominantly generated by ion exchangers, pumps, and channels, proton fluxes across the plasma membrane regulate dynamic changes in cytosolic or intracellular pH (pHi) that contribute to cell proliferation, cytoskeleton remodeling, and glycolytic metabolism (Casey, Grinstein, & Orlowski, 2010; Webb, Chimenti, Jacobson, & Barber, 2011). Proton fluxes across membranes of intracellular organelles generate pH gradients that drive vesicle trafficking and posttranslational modification and sorting of cargo proteins (Marshansky & Futai, 2008; Rivinoja, Kokkonen, Kellokumpu, & Kellokumpu, 2006; Vavassori et al., 2013). Although in normal conditions proton fluxes are homeostatically controlled to maintain pHi and organelle pH within narrow physiological ranges, dysregulated proton fluxes enable many diseases and pathologies, including cancer (Cardone, Casavola, & Reshkin, 2005; Stock & Schwab, 2009; Webb et al., 2011), neurodegenerative disorders (Harguindey, Reshkin, Orive, Arranz, & Anitua, 2007), and a number of myopathies and cardiovascular dysfunctions (Vaughan-Jones, Spitzer, & Swietach, 2009). Our current ability to measure dynamic and localized changes in pH within the cell is facilitated by new generations of pH-sensitive dyes and biosensors. In this chapter, we discuss commonly used fluorescence ratiometric probes, including their properties, uses, advantages, and limitations.

23.1 CURRENTLY USED RATIOMETRIC pH PROBES

Our ability to measure ion fluxes in real time was revolutionized in the 1980s by the development of high-affinity fluorescent Ca^{2+} dyes (Grynkiewicz, Poenie, & Tsien, 1985; Macdonald, Chen, & Mueller, 2012) and H^+ dyes (Paradiso, Tsien, & Machen, 1984; Shaner et al., 2004). The pH-sensitive polar fluorescein derivative 2′,7′-bis-(2-carboxyethyl)-5-(and-6)-carboxyfluorescein, acetoxymethyl ester (BCECF) remains the most widely used pHi indicator. However, experimental limitations imposed by pH-sensitive dyes have more recently led to the development of genetically encoded pH biosensors derived from the jellyfish *Aequorea victoria* green fluorescent

protein (GFP; Martinez et al., 2012; Miesenböck, De Angelis, & Rothman, 1998; Wilks & Slonczewski, 2007). Together, these pH-sensitive dyes and biosensors can be imaged using most standard fluorescence microscopes to measure steady-state and dynamic changes in pH within cells.

23.1.1 pH-SENSITIVE RATIOMETRIC DYES

The pH-sensitive ratiometric dyes BCECF and SNARF-5F 5-(and-6)-carboxylic acid, acetoxymethyl ester, acetate are routinely used to determine pHi in clonal cells and experimentally isolated tissues. The methyl ester moiety makes both dyes membrane-permeant but is cleaved by intracellular esterases, which trap the dyes within cells (Han & Burgess, 2010). The dual-excitation/single-emission dye BCECF has a pH-sensitive excitation at 490 nm (Em 535 nm). The pH-sensitive signal is standardized to dye abundance by pH-insensitive excitation at 440 nm. The dual-emission dye SNARF has pH-sensitive and pH-insensitive emission at 580 and 640 nm, respectively. The ratiometric measurement allows correction for dye leakage out of the cell, photobleaching, and differential dye loading between samples. The interval for optimal dye loading is dependent on cell type and ranges between 10 and 30 min at 37 °C. Of utmost importance is using the minimum dye concentration sufficient for obtaining a fluorescent signal because high dye concentrations can aberrantly sequester protons. In our experience with BCECF, loading 1 μM for 15 min is optimal, with the fluorescent signal lasting $\sim$90 min. For SNARF, we generally use between 2 and 5 μM.

We routinely use SNARF to measure pHi in Chinese hamster lung fibroblasts (ATCC and CCL-39) (Fig. 23.1). In addition to measuring steady-state pH, we also measure the rates of proton efflux by using the NH_4^+ prepulse technique (Boron & De Weer, 1976). Cells incubated with 30 mM NH_4Cl buffer for 5 min have an initial increase in pHi as NH_3 enters the cells and complexes with protons (not shown) until a plateau pHi value is reached (Fig. 23.1, #1). Removing external NH_4Cl causes the pHi to rapidly decrease as NH_3 exits the cell, trapping the protons inside (Fig. 23.1, #2). This acid-loading approach allows measuring the rate of pHi recovery until a plateau is reached (Fig. 23.1, #3) as an index of the activity of ion transport proteins. With corrections for buffering capacity, the flux of proton equivalents can be calculated (Boron & De Weer, 1976). Changes in the rate of pHi recovery can be used to determine the regulation of ion transporter activity, including by growth factors, oncogenes, and extracellular osmolarity. For example, platelet-derived growth factor increases the activity of the plasma membrane Na^+/H^+ exchanger NHE1, as determined by increased pHi recoveries measured in a nominally HCO_3^--free HEPES buffer that prevents the activity of anion exchangers (Meima, Webb, Witkowska, & Barber, 2009). Fluorescence intensities are used to determine ratios that are converted to pH values using a nigericin calibration. Following pH measurement, cells are incubated in a Na^+-free, K^+ buffer containing the ionophore nigericin to equilibrate intracellular and extracellular pH (Thomas, Buchsbaum, Zimniak,
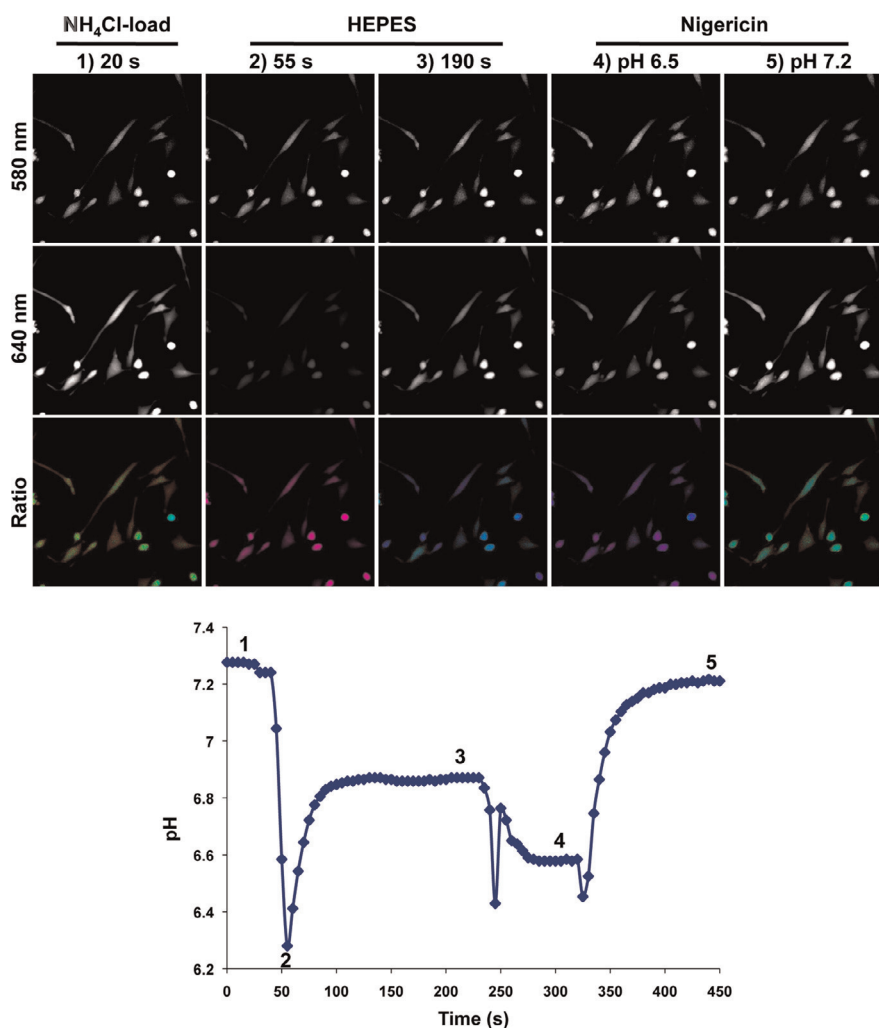
FIGURE 23.1

Using SNARF in CCL-39 fibroblasts to measure pHi recovery from an acid load. Top: Images of SNARF-loaded fibroblasts show the pH-sensitive (580 nm) and pH-insensitive (640 nm) channels and the 580 nm/640 nm ratio. Bottom: Plot of pH versus time calculated from the average 580 nm/640 nm ratio from 10 cells normalized to nigericin buffers of known pH values. See text for details.

& Racker, 1979). The fluorescence ratios obtained with sequential incubations in nigericin-containing buffer adjusted to known pH values are used to generate a calibration curve. Fluorescence ratios with nigericin are generally linear between pH 6.5 and 7.8; hence, we often use a two-point calibration (Fig. 23.1, #4 and #5).

23.1.1.1 Advantages, limitations, and caveats of using dyes

The BCECF and SNARF dyes are easy to use with clonal cells in culture because they do not require transfection or genetic modification to generate new cell lines. They have also been used successfully in some whole-mount tissues (Adams, Tseng, & Levin, 2013; Rossano, Chouhan, & Macleod, 2013). With a pK_a of ~7.0 for BCECF and ~7.5 for SNARF, these dyes are most suitable for measuring cytosolic pH and less effective for measuring pH of acidic intracellular organelles. As described in the preceding text, cleavage of the methyl ester of the AM forms of these dyes is dependent on the activity of intracellular esterases, which can lead to dye accumulation in organelles with high esterase activity. For example, BCECF–AM cannot be used to measure cytosolic pH in the yeast *Saccharomyces cerevisiae* because it accumulates in the yeast vacuole instead of the cytosol, in contrast to cytosolic accumulation in mammalian cells (Plant, Manolson, Grinstein, & Demaurex, 1999). For yeast cells, the genetically encoded pH sensor pHluorin, described in the succeeding text, is more effective for measuring pHi (Brett, Tukaye, Mukherjee, & Rao, 2005). One caveat in mammalian cells is heterogeneous dye uptake (Fig. 23.1). This underscores the importance of including nigericin calibrations with each experiment because dissimilar ratios can reflect variable dye levels rather than actual differences in pHi. Uneven dye loading is a significant problem in some whole-mount tissues, where genetically encoded pH biosensors may be a better approach (see Fig. 23.4). A minimum fluorescence intensity cutoff should be established before ratiometric analysis because ratios will vary significantly as the signal intensity decreases toward the threshold of detection. Metabolism of the dyes, leakage out of the cell, and photobleaching will all decrease the fluorescence intensity over time. Hence, dyes are optimally used for shorter-term measurements of <60 min.

23.1.2 GENETICALLY ENCODED pH SENSORS

Although GFP is pH-sensitive, its pK_a of <6.0 makes it unsuitable for measuring physiological pH in the cytosol and some subcellular compartments and organelles. Two different variants of GFP were first generated by the Rothman laboratory (Miesenböck et al., 1998). Ratiometric pHluorin has a pK_a of ~7.2. Like ratiometric dyes, pHluorin has pH-sensitive fluorescence (410 nm excitation, 510 nm emission) with increased intensity at higher pH and pH-insensitive fluorescence at the isosbestic excitation at 470 nm that can be used to normalize to biosensor abundance. Ecliptic pHluorin has a pK_a of ~7.1 and fluorescence also increases with increasing pH at 410 nm excitation; however, its emission spectrum does not have an isosbestic point to normalize intensity to protein abundance. In more recent studies, this limitation has been addressed by fusing ecliptic pHluorin and pH-insensitive mCherry (Koivusalo et al., 2010). This construct is easy to use with most fluorescence microscopes because ratiometric images can be obtained with GFP and mCherry filter sets, while filter sets for ratiometric pHluorin are distinct. pHluorin constructs have been used to measure pH in the cytosol, at the cell membrane, and in subcellular compartments, including neuronal synapses, the trans-Golgi network, and endosomes
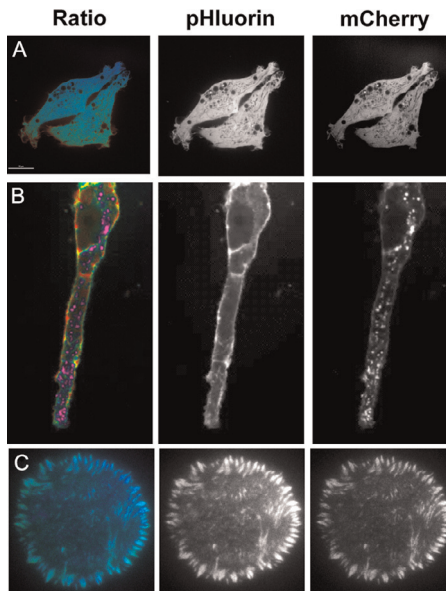
FIGURE 23.2

Targeting mCherry–pHluorin to different subcellular locations allows for the determination of spatially distinct pH. (A) Confocal micrograph of MTLn3 rat mammary adenocarcinoma cells expressing soluble mCherry–pHluorin measured the pH of the cytosol. (B) Confocal micrograph of Madin–Darby canine kidney (MDCK) cells grown in 3D cysts and induced with HGF to form extensions and expressing myristoylated mCherry–pHluorin, which targets the pH sensor to the plasma membrane. Puncta that show mCherry but not pHluorin fluorescence are visible, and these are seen in all cell and tissue samples expressing this pH biosensor. (C) Images of mouse embryonic fibroblast expressing focal adhesion targeting paxillin mCherry–pHluorin imaged by TIRF microscopy.

(Fig. 23.2). For additional information, several excellent reviews describe the use of genetically encoded fluorescent pH sensors (Ashby, Ibaraki, & Henley, 2004; Benčina, 2013; Han & Burgess, 2010; Pinton, Rimessi, Romagnoli, Prandini, & Rizzuto, 2007).

23.1.2.1 Advantages, limitations, and caveats of using genetically encoded pH biosensors

Genetically encoded biosensors have several major advantages. Expression is regulated and hence more homogenous compared with uneven loading of dyes within a cell population. Targeting to specific intracellular locations or subcellular compartments can be achieved, as we show with a paxillin–pHluorin–mCherry construct that localizes to cell-substrate focal adhesions (Fig. 23.2). Additionally, continuous expression of the biosensor allows for live-imaging experiments over a longer timescale than is possible using dyes. Although not currently exploited, whole-animal or tissue-specific expression could be used to image pHi dynamics during

development or disease progression. One caveat of ratiometric imaging is edge ar-
tifacts that can be caused by cell movement between taking the two images
(Fig. 23.2A). In addition, uneven illumination that is different between the two chan-
nels will generate artificial gradients in the ratio image. Thus, ideally, a flat-field
correction should be applied to normalize for uneven excitation. In addition to these
microscopy-induced artifacts, fluorescent protein properties may also give rise to
misinterpretation. For example, accumulations of mCherry-positive, pHluorin-
negative punctae in the cytoplasm of cells and tissue (Fig. 23.2B) may be aggregates
of misfolded protein or represent protein in endosomes or lysosomes where a lower
pH would quench pHluorin fluorescence. For the mCherry–pHluorin fusion protein,
maturation rates of mCherry (~155 min) are slower than pHluorin (GFP, ~15 min)
(Macdonald et al., 2012). Therefore, temporally regulated expression constructs may
show increased ratio as a consequence of immature mCherry. Similarly, without ap-
propriate correction, different rates of photobleaching will result in artificial ratio
changes over time. For example, a total laser exposure time of 108 s results in sig-
nificant photobleaching of a whole-mount *Drosophila* larval eye imaginal disk. This
issue is further complicated when performing ratiometric imaging using mCherry–
pHluorin, as the two fluorescent moieties show different rates of photobleaching
resulting in an apparent change in pHi over time (Fig. 23.3). This underscores the
importance of minimizing exposure of biological samples to light, especially epi-
fluorescence. Several of these limitations can be corrected by calibrating fluores-
cence ratios to pH, as described earlier in the text with nigericin. Nigericin should
equilibrate pH across the entire cell or tissue removing any biological pH gradients,
while ratio differences attributable to imaging artifacts will remain. Different fluo-
rescence ratios do not necessarily reflect different pH values and data should never
be expressed as fluorescent signal intensity or uncalibrated ratios.

23.2 APPLICATIONS
23.2.1 MEASURING pHi IN SINGLE CELLS
23.2.1.1 General considerations
When selecting an appropriate pH indicator, several factors should be considered.
What is the duration of the experiment? While dyes are easy to use, they are lost from
the cell or degraded generally within an hour and are not suitable for long-term ex-
periments. Is the objective to measure pH within the cytosol or within subcellular
organelles? Dyes are most commonly used to determine pH of the cytoplasm and
are difficult to compartmentalize. Genetically encoded sensors can be modified with
targeting sequences to localize to distinct intracellular compartments. The pH of the
region of interest (ROI) should be close to the pK_a of the fluorophore to ensure a
maximum dynamic range. For example, the pH of the mitochondrial matrix is
slightly basic (pH ~7.8), whereas the pH of lysosomes is highly acidic (pH
~4.8). Hence, pK_a values should be considered to choose an indicator that titrates
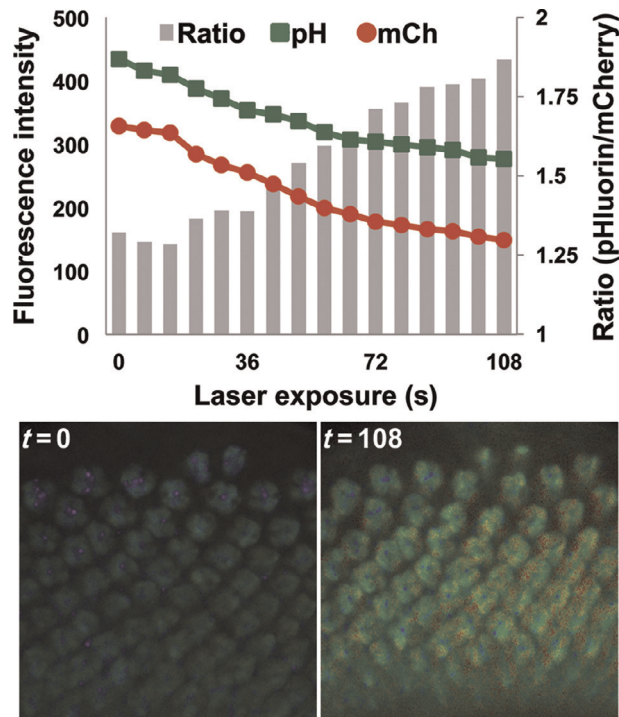within the pH range of the desired cellular compartment.

FIGURE 23.3

Increase of mCherry-pHluorin fluorescence ratio due to different photobleaching rates. Tissue was imaged every 5 s (300 ms exposure) over 30 min for a total laser exposure of 108 s. Following background subtraction, fluorescence intensity was measured at five regions and averaged. Absolute fluorescence intensity values (green squares for pHluorin and red circles for mCherry) after background subtraction decrease at different rates. Ratios are plotted on a secondary Y-axis were generated by dividing pHluorin by mCherry fluorescence values and appear to increase over time due to slower photobleaching of pHluorin compared with mCherry. This is consistent with reported photobleaching rates for GFP (t1/2 1/4115 s) and mCherry (t1/2 1/468 s) (Shaner et al., 2004). One important consequence of photobleaching is that the measured ratio in *Drosophila* eye imaginal disks appears to increase over time (bars and images).

23.2.1.2 Subcellular pH Measurements

As described earlier in the text, the pH of different organelles in the cell maintains distinct pH values, which is required to maintain specific biological processes. The intrinsic buffering capacity protects cellular compartments from rapid changes in pH while pH homeostasis is maintained by the coordinated activity of ion transporters, channels, and pumps. The narrow pH range of the cytosol allows for the optimal activity, stability, structure, and interactions of cytoplasmic macromolecules. The activity of select regulatory proteins, especially enzymes, is sensitive to small physiological changes in pH (Schönichen, Webb, Jacobson, & Barber, 2013), which

should be considered. In general, cytoplasmic pH in most organisms from bacteria (Martinez et al., 2012; Wilks & Slonczewski, 2007) to yeasts (Bagar, Altenbach, Read, & Bencina, 2009; Grynkiewicz et al., 1985) to mammalian cells (Fig. 23.1) is slightly basic (pH is ~7.0–7.8), with the exception of some acidophilic or basophilic bacteria (Paradiso et al., 1984; Slonczewski, Fujisawa, Dopson, & Krulwich, 2009). In contrast, the pH of lysosomes is acidic. Intraorganelle pH gradients are particularly important in the mitochondria. The mitochondria generate ATP by electron transport across the inner membrane coupled to chemiosmotic H^+ translocation from the inner membrane space to the matrix through the ATP synthase. The use of dyes to measure the pH of the mitochondrial matrix or inner membrane space in cells is limited by the inability to separate the mitochondria-specific signal from that of the cytoplasmic background (Chacon et al., 1994; Miesenböck et al., 1998; Porcelli et al., 2005). The development of genetically encoded pH-sensitive fluorescent proteins targeted to the mitochondrial matrix and inner membrane space allows determining mitochondrial pH gradients (Boron & De Weer, 1976; De Michele, Carimi, & Frommer, 2014; Pinton et al., 2007); the pH of the mitochondrial matrix is ~7.78 while the intermembrane space is ~6.88 (Porcelli et al., 2005; Thomas et al., 1979). Further, spontaneous, transient increases in pHi in the mitochondrial matrix, termed "flashes," have been recently observed and likely reflect changes in proton pump activity and the transmembrane H^+ gradient (Han & Burgess, 2010; Schwarzländer, Logan, Fricker, & Sweetlove, 2011; Schwarzländer et al., 2012).

The pH sensitivity of pHluorin has been widely used to determine real-time synaptic vesicle fusion events and endocytosis. When fused to vesicle-specific proteins such as synaptobrevin (Miesenböck et al., 1998), synaptophysin (Granseth, Odermatt, Royle, & Lagnado, 2006), and synaptotagmin (Diril, Wienisch, Jung, Klingauf, & Haucke, 2006), pHluorin localizes to the interior of synaptic vesicles and fluorescence is quenched by low pH (~5.5). With fusion of vesicle and plasma membranes, the pHluorin fluorescent signal rapidly increases. The pHluorin signal decreases again as endocytosis and vesicle acidification occur. This experimental strategy has revealed the kinetics and retrieval of vesicle dynamics (Granseth et al., 2006), vesicle fusion events in motor neurons in *Drosophila* larvae (Denker et al., 2011), and endocytosis *in situ* (Poskanzer, Marek, Sweeney, & Davis, 2003).

pH gradients within the same compartment have also been determined. For example, increased cytosolic pH and decreased extracellular pH at the leading edge of migrating cells are evolutionarily conserved signals necessary for directed cell migration. Experiments using BCECF and SNARF demonstrate that increased pHi promotes *de novo* actin polymerization in a variety of organisms including sea urchin eggs (Begg & Rebhun, 1979), the slime mold *Dictyostelium discoideum* (Patel & Barber, 2005; Plant et al., 1999; Van Duijn & Inouye, 1991), and mammalian cells (Denker & Barber, 2002). More recently, the use of TIRF microscopy using BCECF (Brett et al., 2005; Ludwig, Schwab, & Stock, 2013) and paxillin–mCherry–pHluorin (Fig. 23.2C; Choi, Webb, Chimenti, Jacobson, & Barber, 2013; Miesenböck et al., 1998) reveals an increase of focal adhesion pH during cell migration of mammalian cells. Further, targeting mCherry–pHluorin to the membrane by fusing the probe to

the membrane-targeting sequence of Lyn demonstrated that changes in pH during macropinocytic lamellipodia extension are more profound in the immediate vicinity of the membrane (Koivusalo et al., 2010).

23.2.2 MEASURING pHi IN TISSUES

Early techniques to measure pHi in whole-mount tissues used disruptive patch clamp techniques to monitor electric currents that result from ion exchange across biological membranes. More recently, PET imaging using radiolabeled probes has allowed for estimation of pHi; however, these measurements are imprecise because they rely on stable distribution of the probe that cannot be independently determined. Similar MRI-based techniques show low sensitivity (Miesenböck et al., 1998; Zhang, Lin, & Gillies, 2010). However, with the advent of fluorescent pH probes and quantitative confocal microscopy, it is now possible to accurately measure pHi in whole-mount tissues and *in situ*. Genetically encoded ratiometric pHluorin has been used to determine pHi in intestinal tissue of whole-mount *Caenorhabditis elegans*, where RNAi targeting the Na^+/H^+ exchanger *nhx-2* decreased pHi to ~7.23 compared with ~7.53 in control animals (Granseth et al., 2006; Nehrke, 2003). Also in *C. elegans*, genetically encoded pHluorin was used to measure pHi in the intestine (*nhx-2*, ~7.40), neurons (*cah-4a*, ~7.52), and body wall muscle (*myo-3*, ~7.49) (Diril et al., 2006; Johnson & Nehrke, 2010). BCECF and SNARF were used to measure pHi in *Xenopus* tadpoles (Adams et al., 2013). BCECF and both ratiometric and ecliptic pHluorins were used in *Drosophila* larvae to show that cytoplasmic pHi in motor nerve termini locally decreases with electric stimulation compared with resting conditions (Granseth et al., 2006; Rossano et al., 2013). We have measured pHi in dissected whole-mount tissue from *Drosophila,* including third larval instar imaginal disks and brain, pupal eyes, and wings and adult eyes (Fig. 23.4). We found uneven loading of pH-sensitive dyes, but using transgenic lines expressing UAS–mCherry–pHluorin under the ubiquitous tubulin–GAL4 driver, we obtained fairly homogeneous expression with robust signals amenable to calibration.

23.3 PROTOCOLS
23.3.1 SOLUTIONS

HEPES buffer
    25 mM HEPES
    140 mM NaCl
    5 mM KCl
    10 mM glucose
    1 mM $MgSO_4$
    2 mM $CaCl_2$

Note: pH to 7.4, adjust to volume and add $CaCl_2$ last after bringing almost to volume.
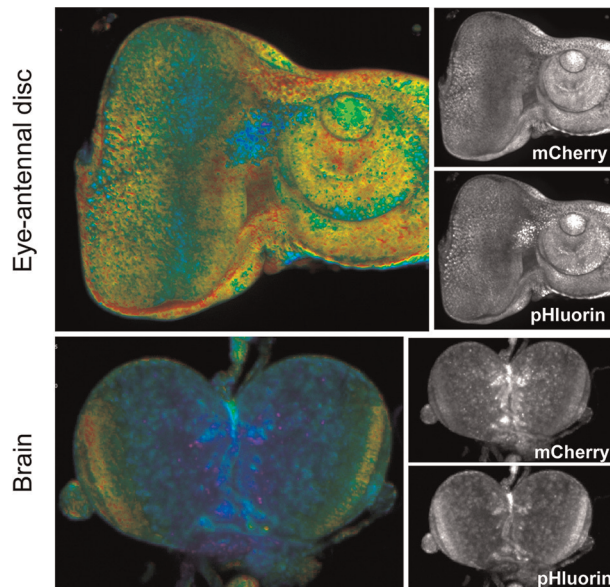
FIGURE 23.4

Determining pHi in whole-mount *Drosophila* tissues using genetically encoded mCherry–pHluorin biosensor. The ubiquitously expressed tubulin–GAL4 driver (Bloomington *Drosophila* Stock Center, # 5138) was used to drive the expression of UAS–mCherry–pHluorin. Tissues were dissected from third instar larvae into HCO_3 buffer and immediately imaged as described in the succeeding text. Ratio images were generated after background subtraction by dividing the fluorescence intensity of the pHluorin signal by the mCherry signal. Eye–antennal imaginal disk (top) and brain show differences in ratio across the tissues.

HCO_3 buffer
25 mM $NaHCO_3$
115 mM NaCl
5 mM KCl
10 mM glucose
1 mM KPO_4 pH 7.4
1 mM $MgSO_4$
2 mM $CaCl_2$

Note: pH to 7.4, adjust to volume and add $CaCl_2$ last after bringing almost to volume.

NH_4Cl buffer
30 mM HEPES
145 mM NaCl
30 mM NH_4Cl
5 mM KCl

10 mM glucose
1 mM KPO_4 pH 7.4
1 mM $MgSO_4$
2 mM $CaCl_2$

Note: pH to 7.4, adjust to volume and add $CaCl_2$ after bringing almost to volume.

Nigericin buffer
25 mM HEPES
105 mM KCl
1 mM $MgCl_2$
Add nigericin to 10 µM (stock is 10 mM in DMSO)
pH with KOH to desired pH points (6.5, 7.0, and 7.5)

Reconstitute 50 µg (one vial with special packaging) BCECF or SNARF (B-1170 and C-1272, Invitrogen) in DMSO to 1 mM. Dilute to working concentrations as indicated in protocols in the succeeding text.

For imaging cells and whole-mount tissues on inverted microscopes, we use 35 mm MatTek glass-bottomed dishes (uncoated, 1.5 mm cover glass; MatTek catalog number P35G-0.170-14-C).

23.3.2 PREPARATION OF CULTURED CELLS

Protocols will vary depending on the cell line being used and optimal conditions must be empirically determined. We describe later in the text a protocol we routinely use for CCL-39 fibroblasts (Fig. 23.1). Fibroblast stocks maintained in growth medium are trypsinized and replated into MatTek imaging dishes 48–72 h before pH measurements. To achieve quiescence, 24 h before use, cells are washed with PBS and maintained in medium with minimal FBS, generally 0.2%. For using dyes, we load cells with 1–5 µM dye for 15 min before use, followed by multiple washes with HCO_3 buffer used for measuring pH. It is important to note that to measure physiological pHi, HCO_3 and not HEPES buffer must be used. For experiments with genetically encoded biosensors, we transfect cells before or after plating in MatTek dishes.

23.3.2.1 Dye loading in cultured cells

Materials required
HEPES buffer
HCO_3 buffer
Nigericin buffers of at least 2 known pH values
NH_4Cl buffer
1 µM BCECF working solution in either tissue culture media without FBS or HCO_3 buffer
Warm solutions to 37 °C prior to the experiment:
(1) Remove culture media from cells.
(2) Wash cells twice with HEPES buffer.

(3) Add 1 ml 1 μM BCECF in HCO_3 buffer to cells. Incubate for 30 min in a 37 °C incubator with 5% CO_2/95% air.

(4) Wash cells twice with HCO_3 buffer. Incubate for 30 min in HCO_3 buffer in a 37 °C incubator to allow for the removal of nonhydrolyzed BCECF from the cells.

(5) After 30 min has elapsed, proceed to imaging the dish as described in the succeeding text.

23.3.2.2 Expression of genetically encoded pH biosensors in cultured cells

There are several methods to express genetically encoded pH biosensors in cells. The easiest method is to transfect the cells with plasmids expressing the biosensor using commercially available transfection reagents. We describe one such protocol later in the text using FuGENE HD to express mCherry–pHluorin in cells 48 h before imaging. Optimal conditions for each cell line and transfection reagent must be empirically determined. Cells that are highly proliferative, such as some cancer cell lines, may need to be transfected in a cell culture dish to drive biosensor expression and repassaged into imaging dishes prior to performing the experiment. For cell lines that are difficult to transfect, an alternative to transfection is to generate a virally encoded biosensor.

Materials required
- PBS solution
- Tissue culture media supplemented with Pen/Strep (basic media)
- Tissue culture media supplemented with FBS and Pen/Strep (complete media)
- FuGENE HD (Promega, catalog number E2311)
- Plasmid encoding a genetically encoded pH biosensor, such as mCherry–pHluorin (Denker et al., 2011; Koivusalo et al., 2010)
- Polypropylene round-bottom tube, 5 ml (Falcon, catalog number 352063)
- Warm media to 37 °C in a water bath before use.
- Warm FuGENE HD to room temperature and vortex before use.
- Cells plated on a MatTek dish, approximately 50–60% confluent at the time of transfection.
- The protocol is sufficient to transfect three 35 mm MatTek dishes:
    (1) For each transfection, add 300 μl of basic media a polypropylene tube.
    (2) Pipette 2 μg plasmid DNA and 8 μl FuGENE HD to the tube.
    (3) Incubate for 15 min at room temperature to complex the DNA.
    (4) Remove culture media from cells.
    (5) Wash twice with 2 ml PBS.
    (6) Add 2 ml fresh complete media and return to the 37 °C incubator.
    (7) After 15 min incubation, add 100 μl of FuGENE HD/DNA mixture to each MatTek dish. Mix by gently swirling the dish. Return cells to the incubator for 24–48 h.
    (8) After 24–48 h, proceed to imaging the dish as described in the succeeding text.

23.3.2.3 Dye loading of whole-mount tissue

We have had variable success dissecting whole tissues and incubating in pH-sensitive dyes. Some tissues showed uneven dye uptake, which made calibration or comparison between samples impossible. Other tissues showed poor dye uptake, such that there was insufficient signal for microscopic detection. Here, altering dye concentration between 5 and 50 μM and increasing incubation up to 60 min may improve signal strength; however, with increased incubation time, tissues will have a relatively shorter viability for imaging and pH calibration.

Materials required
- HCO_3 buffer
- Nigericin buffers of known pH values
- 10 μM BCECF working solution in HCO_3 buffer

Dissection tools
- MatTek dish

(1) Perform dissections of tissue into HCO_3 buffer.
(2) Incubate in 10 μM BCECF in HCO_3 buffer for 30 min in the dark.
(3) Wash tissue twice for 10 min each in HCO_3 buffer.
(4) Mount tissue in MatTek dishes for imaging in HCO_3 buffer. If tissue does not adhere well to the glass bottom, mount in a drop of HCO_3 buffer, and add a coverslip on top to minimize tissue movement after mounting. The coverslip may be secured with nail polish. However, do leave an area open to facilitate buffer exchange for pH calibration step.

23.3.2.4 Expression of genetically coded pH biosensors in genetically tractable organisms

Determination of tissue can be accomplished by using either genetically encoded pH biosensors, such as mCherry–pHluorin. These can be expressed using standard methods for the organism, such as the inducible bipartite GAL4–UAS system in *Drosophila* or as a direct promoter fusion in *C. elegans*:

(1) Perform dissections of tissue into HCO_3 buffer.
(2) Mount tissue in MatTek dishes for imaging in HCO_3 buffer. If tissue does not adhere well to the glass bottom, mount in a drop of HCO_3 buffer, and add a coverslip on top to minimize tissue movement after mounting. The coverslip may be secured with nail polish. However, do leave an area open to facilitate buffer exchange for pH calibration step.

23.3.3 RATIOMETRIC IMAGING

For our analyses, we used an inverted, spinning disk confocal microscope system that was built for live-cell imaging (Poskanzer et al., 2003; Stehbens, Pemble, Murrow, & Wittmann, 2012). For imaging mammalian cells, it is important to have temperature control and to have a constant CO_2 gas supply to support pH homeostasis for the

duration of the experiment. *Drosophila* and *C. elegans* tissue imaging should be performed at ambient temperature.

Acquisition settings should be empirically determined and with the following criteria in mind. First, exposure settings should be as low as possible to prevent photobleaching of samples. Single-fluor sensors (such as BCECF, SNARF, or ratiometric pHluorin) exhibit photobleaching over time, and extended imaging of pH homeostasis may preclude acquisition of accurate calibration curves. Dual-fluor pH sensors (e.g., mCherry–pHluorin) show differential rates of photobleaching (Fig. 23.4). Live-cell TIRF microscopy was performed as described previously (Rossano et al., 2013; Stehbens et al., 2012). Superecliptic pHluorin and mCherry signals were measured using 488 and 561 nm laser illumination, respectively. An initial experiment should be performed to ensure no photobleaching of the two channels occurs. In our hands, TIRF microscopy minimizes the amount of photobleaching observed and signals are stable for hours. At the end of the experiment, a nigericin calibration was performed to normalize pHi values as described later in the text.

23.3.4 GENERATING NIGERICIN CALIBRATION CURVES

Ratiometric pH data are achieved through calibration with a protonophore such as nigericin (Invitrogen, cat # N1495), which equilibrates pHi to buffer pH. By incubating the cell or tissue samples with a nigericin-containing buffer of predetermined pH, ratios can be calibrated to a known pH and a line generated to fit the data across two or three different pH points. It is important to use pH values for calibration that fall within the linear range of the pH sensor (Table 23.1).

Table 23.1 Ratiometric pH Probes for Determining Intracellular pH

Ratiometric pH-sensitive dyes	pH-sensitive wavelength (nm)		pH-insensitive wavelength (nm)		pH range (pK_a)
	Ex	Em	Ex	Em	
BCECF	490	535	440	535	6.4–7.8 (6.98)
SNARF	514	580	514	640	7.0–8.0 (7.5)

Genetically encoded pH biosensors	pH-sensitive wavelength (nm)		pH-insensitive wavelength (nm)		pH range (pK_a)
	Ex	Em	Ex	Em	
Ratiometric pHluorin	410	510	470	535	5.5–7.5 (7.2)
Ecliptic pHluorin	n/a	n/a	475	535	6.0–7.5 (7.1)
mCherry			587	610	(<4.5)

While some groups have used a standard curve to calculate pH data across experiments, we find that it is essential for accuracy and reproducibility to image controls, experimental conditions, and nigericin calibrations on the same day.

Tissues are more susceptible to death upon prolonged nigericin exposure, and severe morphological changes and tissues can disintegrate and make it difficult to generate calibration data for specific regions in tissue. Therefore, we recommend limiting the total time for nigericin incubations of tissues to 30 min.

Protocol
(1) Aspirate buffer and replace with nigericin buffer. Incubate cells for 10 min and tissue samples for 15–30 min.
(2) Image the samples using identical acquisition setting as determined earlier in the text.
(3) Aspirate and replace nigericin buffer. For subsequent buffers, an incubation time of 5 min is usually sufficient.
(4) Repeat as in the preceding text for the remaining calibration point.

23.3.5 RATIOMETRIC ANALYSIS

We perform our ratiometric analysis using the NIS-Elements software to subtract background and extract pixel intensity values and subsequently perform calculations in Microsoft Excel:

(1) Open images in image analysis program. If they are not already, put images from the same sample into a single file to facilitate ROI selection. Select a ROI encompassing only background, and perform background subtraction.
(2) Draw additional ROIs to select samples to calculate pixel intensities. Where appropriate, we often draw a circle and copy and paste to select multiple ROI. Alternately, tracing individual cell features (such as focal adhesions; Choi et al., 2013; Macdonald et al., 2012) may need to be accomplished by hand. When measuring individual cells, we typically select 20–30 cells using individual ROIs, while for tissue measurements, we select 3–5 ROIs per piece of tissue. It is also good to include a background ROI to confirm subtraction.
(3) Export average pixel intensities per ROI from both images into Excel or similar spreadsheet program.
(4) Calculate ratios by dividing the pixel intensity from the pH-sensitive wavelength (e.g., pHluorin) by the pixel intensity from the pH-insensitive wavelength (e.g., mCherry).
(5) Calculate standard curves from nigericin experiments to derive a standard line equation $y = mx + b$. Here, pH values of nigericin buffers will be the y-values, and ratios are the x-values. Solve for the slope and y-intercept.
(6) Take calculated ratios from experimental and control images, and solve the equation for pH value using values calculated previously in the text. Calculated pHi values can be analyzed using appropriate statistical tests.
(7) Images of pH-sensitive to pH-insensitive ratios are pseudocolored with appropriate lookup table (LUT). We use the Rainbow RGB LUT. The scale

should be calibrated using ratios calculated from the nigericin curve. A scale bar labeled with appropriate pH values should be included in the final image. The same scale should be used for all experiments to facilitate comparison across samples.

(8) It is also recommended to include single-channel black and white images for each channel. These images should have the same contrast settings to preserve the difference in signal that reflects different pHi across the sample.

ACKNOWLEDGMENTS

REFERENCES

Adams, D. S., Tseng, A. S., & Levin, M. (2013). Light-activation of the Archaerhodopsin H^+-pump reverses age-dependent loss of vertebrate regeneration: Sparking system-level controls in vivo. *Biology Open, 2*(3), 306–313. http://dx.doi.org/10.1242/bio.20133665.

Ashby, M. C., Ibaraki, K., & Henley, J. M. (2004). It's green outside: Tracking cell surface proteins with pH-sensitive GFP. *Trends in Neurosciences, 27*(5), 257–261. http://dx.doi.org/10.1016/j.tins.2004.03.010.

Bagar, T., Altenbach, K., Read, N. D., & Bencina, M. (2009). Live-cell imaging and measurement of intracellular pH in filamentous fungi using a genetically encoded ratiometric probe. *Eukaryotic Cell, 8*(5), 703–712. http://dx.doi.org/10.1128/EC.00333-08.

Begg, D. A., & Rebhun, L. I. (1979). pH regulates the polymerization of actin in the sea urchin egg cortex. *The Journal of Cell Biology, 83*(1), 241–248.

Benčina, M. (2013). Illumination of the spatial order of intracellular pH by genetically encoded pH-sensitive sensors. *Sensors (Basel), 13*(12), 16736–16758. http://dx.doi.org/10.3390/s131216736.

Boron, W. F., & De Weer, P. (1976). Intracellular pH transients in squid giant axons caused by CO_2, NH_3, and metabolic inhibitors. *The Journal of General Physiology, 67*(1), 91–112, Retrieved from: http://eutils.ncbi.nlm.nih.gov/entrez/eutils/elink.fcgi?dbfrom=pubmed&id=1460&retmode=ref&cmd=prlinks.

Brett, C. L., Tukaye, D. N., Mukherjee, S., & Rao, R. (2005). The yeast endosomal Na+K+/H+ exchanger Nhx1 regulates cellular pH to control vesicle trafficking. *Molecular Biology of the Cell, 16*(3), 1396–1405. http://dx.doi.org/10.1091/mbc.E04-11-0999.

Cardone, R. A., Casavola, V., & Reshkin, S. J. (2005). The role of disturbed pH dynamics and the Na+/H+ exchanger in metastasis. *Nature Reviews. Cancer, 5*(10), 786–795. http://dx.doi.org/10.1038/nrc1713.

Casey, J. R., Grinstein, S., & Orlowski, J. (2010). Sensors and regulators of intracellular pH. *Nature Reviews. Molecular Cell Biology, 11*(1), 50–61. http://dx.doi.org/10.1038/nrm2820.

Chacon, E., Reece, J. M., Nieminen, A. L., Zahrebelski, G., Herman, B., & Lemasters, J. J. (1994). Distribution of electrical potential, pH, free Ca2+, and volume inside cultured adult rabbit cardiac myocytes during chemical hypoxia: A multiparameter digitized

confocal microscopic study. *Biophysical Journal*, *66*(4), 942–952. http://dx.doi.org/10.1016/S0006-3495(94)80904-X.

Choi, C.-H., Webb, B. A., Chimenti, M. S., Jacobson, M. P., & Barber, D. L. (2013). pH sensing by FAK-His58 regulates focal adhesion remodeling. *The Journal of Cell Biology*, *202*(6), 849–859. http://dx.doi.org/10.1083/jcb.201302131.

De Michele, R., Carimi, F., & Frommer, W. B. (2014). Mitochondrial biosensors. *The International Journal of Biochemistry & Cell Biology*, *48*, 39–44. http://dx.doi.org/10.1016/j.biocel.2013.12.014.

Denker, S. P., & Barber, D. L. (2002). Cell migration requires both ion translocation and cytoskeletal anchoring by the Na-H exchanger NHE1. *The Journal of Cell Biology*, *159*(6), 1087–1096. http://dx.doi.org/10.1083/jcb.200208050.

Denker, A., Bethani, I., Kröhnert, K., Körber, C., Horstmann, H., Wilhelm, B. G., et al. (2011). A small pool of vesicles maintains synaptic activity in vivo. *Proceedings of the National Academy of Sciences of the United States of America*, *108*(41), 17177–17182. http://dx.doi.org/10.1073/pnas.1112688108.

Diril, M. K., Wienisch, M., Jung, N., Klingauf, J., & Haucke, V. (2006). Stonin 2 is an AP-2-dependent endocytic sorting adaptor for synaptotagmin internalization and recycling. *Developmental Cell*, *10*(2), 233–244. http://dx.doi.org/10.1016/j.devcel.2005.12.011.

Granseth, B., Odermatt, B., Royle, S. J., & Lagnado, L. (2006). Clathrin-mediated endocytosis is the dominant mechanism of vesicle retrieval at hippocampal synapses. *Neuron*, *51*(6), 773–786. http://dx.doi.org/10.1016/j.neuron.2006.08.029.

Grynkiewicz, G., Poenie, M., & Tsien, R. Y. (1985). A new generation of Ca2+ indicators with greatly improved fluorescence properties. *The Journal of Biological Chemistry*, *260*(6), 3440–3450.

Han, J., & Burgess, K. (2010). Fluorescent indicators for intracellular pH. *Chemical Reviews*, *110*(5), 2709–2728. http://dx.doi.org/10.1021/cr900249z.

Harguindey, S., Reshkin, S. J., Orive, G., Arranz, J. L., & Anitua, E. (2007). Growth and trophic factors, pH and the Na+/H+ exchanger in Alzheimer's disease, other neurodegenerative diseases and cancer: New therapeutic possibilities and potential dangers. *Current Alzheimer Research*, *4*(1), 53–65.

Johnson, D., & Nehrke, K. (2010). Mitochondrial fragmentation leads to intracellular acidification in *Caenorhabditis elegans* and mammalian cells. *Molecular Biology of the Cell*, *21*(13), 2191–2201. http://dx.doi.org/10.1091/mbc.E09-10-0874.

Koivusalo, M., Welch, C., Hayashi, H., Scott, C. C., Kim, M., Alexander, T., et al. (2010). Amiloride inhibits macropinocytosis by lowering submembranous pH and preventing Rac1 and Cdc42 signaling. *The Journal of Cell Biology*, *188*(4), 547–563. http://dx.doi.org/10.1083/jcb.200908086.

Ludwig, F. T., Schwab, A., & Stock, C. (2013). The Na +/H +−exchanger (NHE1) generates pH nanodomains at focal adhesions. *Journal of Cellular Physiology*, *228*, 1351–1358. http://dx.doi.org/10.1002/jcp.24293.

Macdonald, P. J., Chen, Y., & Mueller, J. D. (2012). Chromophore maturation and fluorescence fluctuation spectroscopy of fluorescent proteins in a cell-free expression system. *Analytical Biochemistry*, *421*(1), 291–298. http://dx.doi.org/10.1016/j.ab.2011.10.040.

Marshansky, V., & Futai, M. (2008). The V-type H+-ATPase in vesicular trafficking: Targeting, regulation and function. *Current Opinion in Cell Biology*, *20*(4), 415–426. http://dx.doi.org/10.1016/j.ceb.2008.03.015.

Martinez, K. A., Kitko, R. D., Mershon, J. P., Adcox, H. E., Malek, K. A., Berkmen, M. B., et al. (2012). Cytoplasmic pH response to acid stress in individual cells of *escherichia coli* and bacillus subtilis observed by fluorescence ratio imaging microscopy. *Applied and Environmental Microbiology*, *78*(10), 3706–3714. http://dx.doi.org/10.1128/AEM.00354-12.

Meima, M. E., Webb, B. A., Witkowska, H. E., & Barber, D. L. (2009). The sodium-hydrogen exchanger NHE1 is an Akt substrate necessary for actin filament reorganization by growth factors. *The Journal of Biological Chemistry*, *284*(39), 26666–26675. http://dx.doi.org/10.1074/jbc.M109.019448.

Miesenböck, G., De Angelis, D. A., & Rothman, J. E. (1998). Visualizing secretion and synaptic transmission with pH-sensitive green fluorescent proteins. *Nature*, *394*(6689), 192–195. http://dx.doi.org/10.1038/28190.

Nehrke, K. (2003). A reduction in intestinal cell pHi due to loss of the *Caenorhabditis elegans* Na+/H+ exchanger NHX-2 increases life span. *The Journal of Biological Chemistry*, *278*(45), 44657–44666. http://dx.doi.org/10.1074/jbc.M307351200.

Paradiso, A. M., Tsien, R. Y., & Machen, T. E. (1984). Na+−H+ exchange in gastric glands as measured with a cytoplasmic-trapped, fluorescent pH indicator. *Proceedings of the National Academy of Sciences of the United States of America*, *81*(23), 7436–7440.

Patel, H., & Barber, D. L. (2005). A developmentally regulated Na-H exchanger in Dictyostelium discoideum is necessary for cell polarity during chemotaxis. *The Journal of Cell Biology*, *169*(2), 321–329. http://dx.doi.org/10.1083/jcb.200412145.

Pinton, P., Rimessi, A., Romagnoli, A., Prandini, A., & Rizzuto, R. (2007). Biosensors for the Detection of Calcium and pH. *Methods in Cell Biology*, *80*, 297–325. http://dx.doi.org/10.1016/S0091-679X(06)80015-4.

Plant, P. J., Manolson, M. F., Grinstein, S., & Demaurex, N. (1999). Alternative mechanisms of vacuolar acidification in H(+)-ATPase-deficient yeast. *The Journal of Biological Chemistry*, *274*(52), 37270–37279, Retrieved from: http://eutils.ncbi.nlm.nih.gov/entrez/eutils/elink.fcgi?dbfrom=pubmed&id=10601292&retmode=ref&cmd=prlinks.

Porcelli, A. M., Ghelli, A., Zanna, C., Pinton, P., Rizzuto, R., & Rugolo, M. (2005). pH difference across the outer mitochondrial membrane measured with a green fluorescent protein mutant. *Biochemical and Biophysical Research Communications*, *326*(4), 799–804. http://dx.doi.org/10.1016/j.bbrc.2004.11.105.

Poskanzer, K. E., Marek, K. W., Sweeney, S. T., & Davis, G. W. (2003). Synaptotagmin I is necessary for compensatory synaptic vesicle endocytosis in vivo. *Nature*, *426*(6966), 559–563. http://dx.doi.org/10.1038/nature02184.

Rivinoja, A., Kokkonen, N., Kellokumpu, I., & Kellokumpu, S. (2006). Elevated Golgi pH in breast and colorectal cancer cells correlates with the expression of oncofetal carbohydrate T-antigen. *Journal of Cellular Physiology*, *208*(1), 167–174. http://dx.doi.org/10.1002/jcp.20653.

Rossano, A. J., Chouhan, A. K., & Macleod, G. T. (2013). Genetically encoded pH-indicators reveal activity-dependent cytosolic acidification of Drosophila motor nerve termini in vivo. *The Journal of Physiology*, *591*(Pt 7), 1691–1706. http://dx.doi.org/10.1113/jphysiol.2012.248377.

Schönichen, A., Webb, B. A., Jacobson, M. P., & Barber, D. L. (2013). Considering protonation as a posttranslational modification regulating protein structure and function. *Annual Review of Biophysics*, *42*, 289–314. http://dx.doi.org/10.1146/annurev-biophys-050511-102349.

Schwarzländer, M., Logan, D. C., Fricker, M. D., & Sweetlove, L. J. (2011). The circularly permuted yellow fluorescent protein cpYFP that has been used as a superoxide probe is highly responsive to pH but not superoxide in mitochondria: Implications for the existence of superoxide 'flashes'. *Biochemical Journal*, *437*(3), 381–387. http://dx.doi.org/10.1042/BJ20110883.

Schwarzländer, M., Murphy, M. P., Duchen, M. R., Logan, D. C., Fricker, M. D., Halestrap, A. P., et al. (2012). Mitochondrial "flashes": A radical concept repHined. *Trends in Cell Biology*, *22*(10), 503–508. http://dx.doi.org/10.1016/j.tcb.2012.07.007.

Shaner, N. C., Campbell, R. E., Steinbach, P. A., Giepmans, B. N. G., Palmer, A. E., & Tsien, R. Y. (2004). Improved monomeric red, orange and yellow fluorescent proteins derived from Discosoma sp. red fluorescent protein. *Nature Biotechnology*, *22*(12), 1567–1572. http://dx.doi.org/10.1038/nbt1037.

Slonczewski, J. L., Fujisawa, M., Dopson, M., & Krulwich, T. A. (2009). Cytoplasmic pH measurement and homeostasis in bacteria and archaea. *Advances in Microbial Physiology*, *55*, 1–317. http://dx.doi.org/10.1016/S0065-2911(09)05501-5.

Stehbens, S., Pemble, H., Murrow, L., & Wittmann, T. (2012). Imaging intracellular protein dynamics by spinning disk confocal microscopy. *Methods in Enzymology*, *504*, 293–313. http://dx.doi.org/10.1016/B978-0-12-391857-4.00015-X.

Stock, C., & Schwab, A. (2009). Protons make tumor cells move like clockwork. *Pflügers Archiv/European Journal of Physiology*, *458*(5), 981–992. http://dx.doi.org/10.1007/s00424-009-0677-8.

Thomas, J. A., Buchsbaum, R. N., Zimniak, A., & Racker, E. (1979). Intracellular pH measurements in Ehrlich ascites tumor cells utilizing spectroscopic probes generated in situ. *Biochemistry*, *18*(11), 2210–2218, Retrieved from: http://eutils.ncbi.nlm.nih.gov/entrez/eutils/elink.fcgi?dbfrom=pubmed&id=36128&retmode=ref&cmd=prlinks.

Van Duijn, B., & Inouye, K. (1991). Regulation of movement speed by intracellular pH during Dictyostelium discoideum chemotaxis. *Proceedings of the National Academy of Sciences of the United States of America*, *88*(11), 4951–4955, Retrieved from: http://eutils.ncbi.nlm.nih.gov/entrez/eutils/elink.fcgi?dbfrom=pubmed&id=11607188&retmode=ref&cmd=prlinks.

Vaughan-Jones, R. D., Spitzer, K. W., & Swietach, P. (2009). Intracellular pH regulation in heart. *Journal of Molecular and Cellular Cardiology*, *46*(3), 318–331. http://dx.doi.org/10.1016/j.yjmcc.2008.10.024.

Vavassori, S., Cortini, M., Masui, S., Sannino, S., Anelli, T., Caserta, I. R., et al. (2013). A pH-regulated quality control Cycle for surveillance of secretory protein assembly. *Molecular Cell*, *50*(6), 783–792. http://dx.doi.org/10.1016/j.molcel.2013.04.016.

Webb, B. A., Chimenti, M., Jacobson, M. P., & Barber, D. L. (2011). Dysregulated pH: A perfect storm for cancer progression. *Nature Reviews. Cancer*, *11*(9), 671–677. http://dx.doi.org/10.1038/nrc3110.

Wilks, J. C., & Slonczewski, J. L. (2007). pH of the cytoplasm and periplasm of *Escherichia coli*: Rapid measurement by green fluorescent protein fluorimetry. *Journal of Bacteriology*, *189*(15), 5601–5607. http://dx.doi.org/10.1128/JB.00615-07.

Zhang, X., Lin, Y., & Gillies, R. J. (2010). Tumor pH and its measurement. *Journal of Nuclear Medicine*, *51*(8), 1167–1170. http://dx.doi.org/10.2967/jnumed.109.068981.